HHS Public Access

Author manuscript

World Neurosurg. Author manuscript; available in PMC 2015 November 01.

Published in final edited form as:

World Neurosurg. 2014 November ; 82(5): 684–695. doi:10.1016/j.wneu.2013.08.029.

Mechanisms of Endothelial Cell Attachment, Proliferation, and Differentiation on 4 Types of Platinum-Based Endovascular Coils

Aditya S. Pandey[1], **James D. San Antonio**[2], **Sankar Addya**[3], **Saul Surrey**[4], **Paolo Fortina**[3,6], **Elisabeth J. Van Bockstaele**[5], and **Erol Veznedaroglu**[7]

[1]Department of Neurosurgery, University of Michigan, Ann Arbor, Michigan, USA

[2]Operations, Stryker Corporation, Malvern, Pennsylvania, USA

[3]Department of Cancer Biology, Cancer Genomics Laboratory, Kimmel Cancer Center, Thomas Jefferson University, Jefferson Medical College, Philadelphia, Pennsylvania, USA

[4]Department of Medicine, Cardeza Foundation for Hematologic Research, Thomas Jefferson University, Jefferson Medical College, Philadelphia, Pennsylvania, USA

[5]Department of Neurosurgery, Thomas Jefferson University, Jefferson Medical College, Philadelphia, Pennsylvania, USA

[6]Department of Molecular Medicine, University La Sapienza, Rome, Italy

[7]Stroke and Cerebrovascular Center of New Jersey, Capital Health System, Trenton, New Jersey, USA

Abstract

OBJECTIVE—A subarachnoid hemorrhage is neurologically devastating, with 50% of patients becoming disabled or deceased. Advent of Guglielmi detachable coils in 1995 permitted endovascular treatment of cerebral aneurysms. Coiling is efficacious and safe, but durability needs improvement, as nearly 20% of patients require further invasive intervention secondary to aneurysm recurrence. The aim of this study is to develop an in vitro model of endothelial cell (EC) proliferation and differentiation on four types of platinum-based coils, using gene expression profiling to understand EC biology as they colonize and differentiate on coils.

METHODS—Human umbilical vein ECs were grown in vitro on platinum coil segments. Growth patterns were assessed as a function of coil type. Gene expression profiles for coil attached versus coil unattached ECs were determined using immunohistochemistry and gene array analysis.

RESULTS—ECs showed rapid, robust attachment to all coil types. Some detachment occurred within 24–48 hours. Significant growth of remaining attached cells occurred during the next week,

To whom correspondence should be addressed: Aditya S. Pandey, M.D., adityap@med.umich.edu.

Conflict of interest statement: This work was supported in part by a grant from the National Institutes of Health within the Department of Cancer Biology (SA and PF) at the Kimmel Cancer Center, Thomas Jefferson University, the Cardeza Foundation for Hematologic Research at Jefferson Medical College (SS), the Department of Neurosurgery at Thomas Jefferson Hospital, and Covidien, Mansfield, MA.

creating a confluence on coils and within coil grooves. Similar growth curve results were obtained with human brain ECs on platinum-based coil surfaces. Differentiation markers in attached cells (α_1, α_2, β_1 integrins) were expressed on immunostaining, whereas microarray gene expression revealed 48 up-regulated and 68 down-regulated genes after 24-hour growth on coils. Major pathways affected as a function of time of colonization on coils and coil type included those involved in regulation of cell cycle and cell signaling.

CONCLUSIONS—We developed an in vitro model for evaluating endothelialization of platinum coils to optimize coil design to support robust EC colonization and differentiation.

Keywords

Cerebral aneurysms; Coils; Endothelial cells; Subarachnoid hemorrhage; Tissue engineering

INTRODUCTION

Thirty-five thousand patients suffer from aneurysmal subarachnoid hemorrhage yearly within the United States. The International Subarachnoid Aneurysm Trial (ISAT) reported a lower probability of death and disability for patients undergoing coiling of cerebral aneurysms as opposed to micro-surgery (15). Although ISAT built the platform for launching endovascular treatment of cerebral aneurysms as a mainstay therapy, the durability of this treatment method remains inferior to that of microsurgery. Based on follow-up cerebral angiography, 10%–30% of all coiled aneurysms will show recurrence (1, 18). Recurrence of coiled aneurysms leads to increased morbidity secondary to retreatments, angiographic follow-up, and the real risk of rerupture.

The goal of endovascular occlusion of aneurysms is to introduce platinum-based coils into the cerebral aneurysm until the entire aneurysm volume is filled with thrombus and coils. Volumetric analysis shows that most aneurysms are only filled 20%–40% with coils, and the rest represents acute thrombus (1). Histopathologic analyses based on autopsy of patients who harbored coiled aneurysms show that within the first 4 weeks, the aneurysm houses organized thrombus, which then develops into minimal fibrous tissue. Endothelial proliferation seems to occur at 3 months after embolization (3, 4, 21). At 12 months after the procedure, coils seem to be embedded in fibrous tissue with endothelialization occurring over the neck of the aneurysm (3, 4, 21). Recurrence takes place when the endothelialization process does not occur across the neck of the aneurysm and thus, the pulsatility is transmitted to the coil/thrombus mass leading to coil compaction as the thrombus dissolves. Our goal is to understand the interaction of platinum coils with endothelial cells (ECs), with the future aim of creating an intra-aneurysmal environment for EC proliferation across the neck of the aneurysm.

MATERIALS AND METHODS

Endovascular Coils

To facilitate growth curves, we purchased the following coils: Guglielmi detachable coils (GDCs) and Matrix coils from Boston Scientific, Natick, Massachusetts, USA; Cerecyte coils from Micrus Endovascular, San Jose, California, USA; and HydroCoils from

MicroVention, Tustin, California, USA. Coil fragments measured 1 cm (each was weighed using an analytical balance), and were used for cellular attachment, growth analysis, immunohistochemistry, and gene array analysis.

Human Umbilical Vein EC Isolation

Umbilical cords were obtained from the Labor and Delivery Department, Thomas Jefferson University Hospital, Philadelphia, Pennsylvania, USA. Human umbilical vein ECs (HUVEC) were isolated from the cords using a collagenase digestion protocol, as described previously (9).

Cell Culture

HUVEC were cultured on tissue culture flasks coated with 0.2% gelatin. Cells were fed a complete media consisting of Media 199 (GIBCO, Carlsbad, California, USA), 10% fetal bovine serum (FBS; HyClone, Logan, Utah, USA), 50 μg/mL EC growth supplement, 50 μg/mL heparin sodium salt from porcine intestinal mucosa (Grade I-A; Sigma-Aldrich, St. Louis, Missouri, USA), 1% penicillin-streptomycin (GIBCO), and 0.1% Fungizone (GIBCO). EC growth supplement was isolated from bovine hypothalami, as described previously (12). HUVECs were used through passage 6. Similar growth curve experiments were also performed with human cerebral microvascular ECs (hCMEC/D3) at less than 10 passages (27). These cells were cultured for 2 weeks to reach confluency, at which time they were trypsinized and diluted to 1,000,000 cells/mL for experimentation. Similar cellular media, warming tray, and techniques were used for the growth curve assessment.

EC Seeding of Endovascular Coils

EC were trypsinized from confluent cultures and 1.0 mL of a 1×10^6 cells/mL suspension was placed in a sterile Eppendorf tube. One coil segment (~1 cm) was added to each tube and the weight measured. Samples were then placed in a tissue culture incubator on a rocking platform for 4–6 hours, and were gently rotated to ensure cell contact with the coil. Coils were then removed from the cell suspension and rinsed by dipping them once into a well of a 12-well tissue culture plate containing Hanks balanced salt solution at 2 mL/well. Coils were then placed into complete media in a 12-well tissue culture plate and returned to the tissue culture incubator. Culture medium was replaced every 2 days thereafter.

Measurement of EC Growth on Coils

At various times during culture (typically at days 1, 3, 7, 14, and 28), cells were removed from the coils by trypsinization and counted. Coils were placed in 0.5 mL trypsin/coil for 5–10 minutes; the resultant cell suspension was mixed 1:1 with complete media to neutralize the trypsin. Cells released from the coils were counted using a hemacytometer, and expressed as cells bound/milligram of coil. Micrographs of cell-populated coils were also taken before and after trypsinization using inverted microscopy.

Immunohistochemical Staining of EC-populated Coils

After ECs proliferated on GDCs for 7 days, coil segments and unattached cells that had become confluent within the wells were fixed using 10% buffered formalin. These two

populations (attached and unattached cells) were incubated with primary anti-bodies to α_1 integrin, α_2 integrin, β_1 integrin, or platelet EC adhesion molecule overnight at 4°C. Samples were labeled with fluorescein isothiocyanate-conjugated secondary antibodies and imaged using fluorescent microscopy.

Examination of EC Gene Expression by Gene Array Analysis

Total RNA Isolation—DNA-free total RNA of cultured cells was isolated using the RNeasy Micro Kit (Qiagen, Valencia, California, USA) according to manufacturer's instructions. In brief, 1×10^5 cells from duplicate cultures (control and experimental) were pelleted, lysed in RNA lysis tissue buffer containing 1% (vol/vol) β-mercaptoethanol. DNase-treated RNA was ethanol precipitated and quantified on a NanoDrop ND-1000 spectrophotometer (Thermo Fisher Scientific, Waltham, Massachusetts, USA), followed by RNA quality assessment by analysis on an Agilent 2100 bioanalyzer (Agilent Technologies, Palo Alto, California, USA).

Microarray Methods—Ribo-single-primer-isothermal-amplification-based RNA amplifications and target preparations were performed according to the manufacturer's instructions (Ovation Biotin System; NuGEN Technologies, San Carlos, California, USA). Briefly, first-strand complementary DNA (cDNA) was synthesized from 50 ng of total RNA using reverse transcription with a unique oligo (dT)/RNA chimeric primer. In the second step, DNA/RNA heteroduplex double-strand cDNA was generated with DNA polymerase. In the third step, SPIA linear isothermal DNA amplification process was performed using DNA/RNA chimeric primer, DNA polymerase, and RNase H in a homogenous isothermal assay that provides efficient amplification of DNA sequence.

Fragmentation and Biotin Labeling—In the first step, DNA amplification products were fragmented by chemical and enzymatic fragmentation that yields single-stranded cDNA products in the 50- to 100-base range. In the second step, fragmented product is labeled by enzymatic attachment of a biotin-labeled nucleotide to the 3-hydroxyl end of the fragmented cDNA.

Hybridization and Bioinformatic Analysis of Messenger RNA Expression Profiling—Fragmented and biotin-labeled target (3.75 μg) in 200 μL of hybridization cocktail was used for each Affymetrix HG U133 Plus 2.0 array (Affymetrix, Santa Clara, California, USA), which contains 56,000 probe sets representing 34,000 well-characterized human genes. Target denaturation was done at 99°C for 2 minutes, and hybridization was performed for 18 hours. Arrays were washed and stained using GeneChip Fluidic Station 450, and hybridization signals were amplified using antibody amplification with goat IgG (Sigma-Aldrich) and anti-streptavidin biotinylated antibody (Vector Laboratories, Burlingame, California, USA). Chips were scanned on an Affymetrix GeneChip Scanner 3000 using GeneChip Operating Software version 3.0. A flow-chart analysis is shown in Figure 1. Normalization was accomplished using robust multi-array average to arrive at baseline transformation for the median of all samples using GeneSpring GX version 10.0 software (Agilent). The gene list was filtered by removing low expressers (<100 signal value in all four samples). A volcano plot was used to identify differentially expressed genes (DEGs)

using unpaired *t*-test with no multiple testing correction (condition, $P = 0.05$, and twofold change).

Gene Annotation—Expressed and DEG lists were linked to the genome database NetAffx at the NetAffx Analysis Center (http://www.affymetrix.com) using Microsoft Excel and Microsoft Access. Gene ontology functions and pathway analysis were assigned using database for Annotation, Visualization, and Integrated Discovery (DAVID version 2.0; http://david.abcc.ncifcrf.gov/). The DEG list was used to perform biological network and functional analysis using Ingenuity Pathway Analysis (IPA) software version 5.0 (Ingenuity Systems Inc., Redwood City, California, USA).

RESULTS

EC Attachment and Proliferation on Platinum-Based Coils

Upon incubation of ECs with platinum coil segments, anywhere from 2000 to 12,000 cells attached for every milligram of coil segment. The cells appeared to attach as clusters, and during the next 24 hours most cells within the clusters appeared to detach as aggregates. Within the first 24 hours, there was an approximate 20% loss of cells, but during the next 96 hours there was an approximate 60% increase in the number of cells associated with the coils, confirming EC proliferation on platinum coils (Figure 1A, B). This increase in cell numbers continued until days 10–15 when there were 7000–10,000 cells per milligram of coil (Figure 1C). After this time and during the next week, there was a reduction in the number of coil-bound cells (Figure 2A). The same phenomenon was observed for human brain EC growth on platinum-based coil surfaces (Figure 2C).

Cellular Attachment and Proliferation on Coated Coils

GDCs, HydroCoils, Matrix coils, and Cerecyte coils all had similar numbers of ECs attaching during the incubation period (300–850 cells/mg of coil). Within the first 72 hours, 200–400 ECs/mg of coil segment remained. During the next 4 days there was marked cell proliferation on the Cerecyte coils (~1400 cells/mg coil) and HydroCoils (~1750 cells/mg coil); however, cell numbers on the GDCs (600 cells/mg coil) and Matrix coils (100 cells/mg coil) were constant with no evidence of proliferation (Figure 2B). During the next week, cellular proliferation occurred on the Cerecyte coils (~2850 cells/mg coil) and the GDCs (~1600 cells/mg coil), remained stable on the HydroCoils (~1800 cells/mg coil), and showed no evidence of proliferation on the Matrix coil (~500 cells/mg coil).

Immunohistochemistry

Figure 1 shows EC attachment to coil segments, and evidence of cellular proliferation and their colonization within coil crevices. Immunohistochemical staining for EC adhesion/signaling receptors α_1 integrin, α_2 integrin, β_1 integrin, and platelet EC adhesion molecule showed diffuse staining of cells when attached to coil segments, or when grown on tissue culture plastic in the absence of coils (Figure 3).

Microarray Analyses of ECs Grown in Culture with or without a Coil

Transcriptome analyses were performed by genomewide microarray expression profiling to define expressed and DEGs after 24-hour growth of ECs in the presence versus absence of a coil. A flow chart for microarray analysis is shown in Figure 4. Array data reproducibility was documented by comparison of a linear scatter plot of spot intensities at each register on duplicate arrays using RNA derived from two replicate control cultures grown in the absence of a coil (Figure 5; slope =1.0136, R^2 =0.9892). When average signal values <100 were excluded, 11,894 probe sets (7929 unique genes) were expressed from duplicate untreated cultures. This represents 21.8% of arrayed probe sets (11,894/54,675) and corresponds to 7929 unique genes. The number of expressed probe sets showed minimal change when comparing control to coil-grown cultures. Many of the highest values were messenger RNAs coding for ribosomal proteins, thymosin beta 10, β-actin, eukaryotic translation elongation factor 1 α_1, ferritin light chain, cytochrome c oxidase subunit II, tubulin, α_1B, and annexin A2.

Identification of DEGs after 24-Hour Growth of ECs

Using signal intensities >100 in at least one of the four samples and ≥2-fold up or down as the criterion for definition of a DEG, we next performed a volcano plot analysis to compare the two replicate controls against the two cultures grown on the coil (Figure 6, *left*). Such a plot defines fold change (x-axis) as a function of statistical significance (y-axis). This analysis identified 135 probe sets at a *P* value of 0.05 (red dots), which were differentially expressed as a result of EC growth on the coil. This included 58 probe sets (48 genes) that were up-regulated and 77 (68 genes) that were down-regulated in response to growth on the coil (Tables 1 and 2). A heat map shows up-regulated and down-regulated genes for duplicate cultures (Figure 6, *right*). Seventy-one of 77 down-regulated probe sets belong to functional categories. Functional categories include phosphoprotein metabolism [42], cell division [12], cell cycle [15], mitosis [10], DNA replication [4], cell cycle control [3], and metal binding [2]. *Kyoto Encyclopedia of Genes and Genomes* pathway analysis shows “cell cycle” as the major affected pathway containing four different genes (cyclin A1, cell division control protein 6 homolog, cell division cycle 25C splice variant 3, and extra spindle poles-like 1 protein) designated as down-regulated in ECs in response to growth on the coil.

A functional annotation chart also is given for the 58 up-regulated probe sets demonstrating 50 belong to different functional categories: signal [26], glycoprotein [27], transmembrane [20], membrane [22], secreted [10], extracellular [4], and receptor [9]. KEGG pathway analysis shows “cytokine-cytokine receptor interaction” as the major affected pathway containing four different genes (C-C motif chemokine 2 precursor, oncostatin M receptor, tumor necrosis factor, and leptin receptor) up-regulated in response to growth on the coil.

Biological Network and Functional Analysis

To further refine the functional properties of the DEGs, all 134 genes were analyzed in the IPA tool for network, functional, and pathway analysis. IPA converts a list of genes with accompanying expression information into a set of relevant networks based on the Ingenuity Knowledge Base pathways. A core analysis is performed for the list of genes. The genes

were categorized based on molecular function in the IPA software. The identified genes also were mapped to molecular networks in the IPA database and ranked by score. The score reflects the probability that a collection of genes equal to or greater than the number in a network could be achieved by chance alone. The top five (high score) networks are listed in Table 3. Network analysis revealed two important networks related to cellular function and cell-to-cell signaling (Figure 7). Two networks have high scores of 40 and 30, with 20 and 16 focus genes, respectively. Several important genes, such as CCNA1, BUB1B, CDC6, CDC25c, A2M, SULF1, TNFSF10, and TXN1P are related in the network. Further molecular and cellular functional classifications are listed in Table 4, showing that 26 genes are related to cell cycle (4 molecules are up-regulated and 22 genes are down-regulated) and 19 genes are related to cell-to-cell signaling interaction function (14 genes are up-regulated and 5 are down-regulated).

DISCUSSION

Cerebral aneurysmal rupture leads to significant morbidity and mortality (21). Endovascular occlusion of aneurysms is a safe and efficacious treatment modality as supported by the ISAT; however, recurrence of previously coiled aneurysms occurs in 10%–30% of patients (15, 18). Endothelialization across the neck of an aneurysm is essential in preventing such recurrence and associated complications (5, 6, 22). The role of ECs in aneurysmal healing after coiling is essential, as these cells are involved in control of vascular tone, thrombosis, thrombolysis, and platelet activation regulation (2, 7, 28). To evaluate the interaction of ECs with platinum-based coils, we developed an in vitro model by seeding coils with HUVECs and examining their proliferation and gene expression profiles.

We observed cellular attachment to coil segments within hours of incubation. Most adherent cells then detached from the coils as aggregates. During the next 7–14 days, cellular proliferation continued until a confluent population of ECs was observed on coil segments. Cell populations could also be observed within the coil segment grooves—a potentially ideal location, as the cells were protected from shear stress associated with flow within the wells. Intercellular contact on the coil segment as well as EC differentiation could have led to inhibition of cellular proliferation as well as cellular death; thus, the observed decrease in number of attached cells in the third week after attachment (25).

With the introduction of different coil types to the clinical market, we evaluated HUVEC attachment and growth pattern on these modified coil fragments. GDCs are unmodified platinum coils and have been used as the control in these experiments. Matrix coils have a polyglycolic acid (PGLA) coating on the platinum surface as opposed to Cerecyte coils that have a PGLA coating within the platinum core (8, 11). HydroCoils have a hydrogel coating on the platinum surface, which allows for volumetric enlargement when the coils are hydrated within an in vivo system (14, 16). A similar number of cells attached to each coil type; however, the greatest proliferation occurred on Cerecyte coils, followed by HydroCoils and GDCs. Matrix coil segments supported the least proliferation, which could be secondary to the PGLA coating being in direct contact with the HUVECs. HydroCoil enlargement leads to an increase in surface area; thus, more potential space for cellular proliferation

without intercellular inhibition, which could explain the larger number of HUVEC cells colonizing this coil type.

Immunohistochemical analysis with antibody labeling for α_1, α_2, and β_1 integrins revealed similar labeling of cells to the coil segments compared with unattached cells (14). Thus, these represent functional HUVECs, as they do not seem to change their cellular membrane integrity when attaching and proliferating on GDC segments (10, 26). In addition, labeling revealed the confluence of cellular proliferation on the coil segments as well as within the crevices of the coils. We analyzed the gene expression of cells attached to the platinum coils versus those grown on tissue culture plastic in the absence of coils, and found that 48 genes were up-regulated whereas 68 genes were down-regulated. The dominating cellular function of down-regulated genes involved cell cycle regulation, whereas genes up-regulated mostly involved cytokine-to-cytokine interaction. The platinum surface most certainly decreased cellular proliferation compared with cells grown in wells. Thus, down-regulation of cell cycle-associated genes was expected and confirmed by our microarray expression studies. It is feasible that EC differentiation could be occurring sooner on the platinum surfaces, leading to a down-regulation of proliferation-associated genes and decreased growth rates on the platinum-based surfaces. Coil segments could also initiate an inflammatory response from the HUVECs, as cytokine-related genes were differentially up-regulated within the attached cellular population (20).

Ozawa et al. (17) and Tamatani et al. (23, 24) reported that canine ECs require extracellular matrix (ECM; fibronectin, laminin, collagen) coating on embolic material for cellular proliferation. They did not observe EC proliferation on uncoated embolic materials. They concluded that ECs require ECM for attachment, growth, and proliferation. Our in vitro model uses HUVECs and achieves cellular attachment, growth, and proliferation on bare platinum as well as PGLA-coated coils. However, it is possible that culture media-derived growth and differentiation factors (e.g., plasma fibronectin) may adhere to the coil surfaces in our model system, creating an ECM-like surface.

Most investigators have reported that collagen type I represents the most ideal substrate for EC proliferation (13). Although collagen provides the appropriate extracellular support for attachment and proliferation, it is also thrombogenic and thus could pose significant thromboembolic risk in the event that coils are coated with this material. In theory, allowing for cellular proliferation on uncoated material would be ideal in reducing the probability of thrombogenicity, as well as allowing for permanent healing within the aneurysm.

We also evaluated the growth of human brain ECs (hCMEC/D3) on different coil types to understand whether brain ECs would have different growth curves on the platinum surfaces compared with HUVECs (27). The overall growth curve is similar to what we observed for HUVECs, as there is exponential growth during the first 7–10 days after cellular attachment. After confluency was reached in the first 10 days, there was a decrease in cell numbers at 2–3 weeks after attachment secondary to cellular growth inhibition, secondary to a lack of surface area. We were not able to detect a statistically significant difference in the number of cells present on the different coil types.

The in vitro model for EC interaction with coils reported here could be used to identify factors to enhance cellular attachment and proliferation in an in vivo situation. In addition, it could serve as the initial step in tissue engineering, as a mechanism for permanent healing within cerebral aneurysms. Tissue engineering requires cellular harvest, attachment to a matrix, and proliferation. The platinum coil could serve as the scaffold, with the goal of attaching smooth muscle cells to endothelium-coated coils with the aim of introducing functional endothelial and smooth muscle cells into the aneurysm lumen (29). Although these cells were able to attach and proliferate when placed on a rocker causing continuous motion, we do aim to modify our in vitro design to introduce calculated flow rates as would be present in an in vivo situation.

Based on our results, we propose a model for the endothelialization of coils: 1) cells attach loosely to the outermost surface of the coil; 2) loosely adherent cells detach; and 3) strongly adherent cells then migrate or compact within flow-protected area of the coil surface (i.e., in the grooves between coil wires). Our results suggest that coils may have the innate capacity to foster EC growth and interactions. These results could be used for development of coils optimized for EC seeding and growth with their surface profile configured with grooves to facilitate attachment and growth of parallel lines of ECs (as has been done for vascular stents) (19). Increasing the surface area-to-volume ratio, as well as decreasing the distance between metallic surfaces within the coil grooves to 10–20 μm (the diameter of ECs), could optimize cellular migration and proliferation. Optimizing EC colonization of coils with biological as well as mechanical modifications should result in endogenous endothelialization within weeks of coil introduction and thus, prevent recurrence as well as need for long-term anticoagulation.

CONCLUSIONS

EC proliferation across the neck of an aneurysm plays a critical role in the formation of permanent healing and prevention of recurrence in previously coiled aneurysms. Our in vitro model of HUVEC and human brain EC attachment and proliferation on coil segments advances toward the goal of rational design of platinum-based coils to support optimal growth and differentiation of ECs, thus potentially enhancing coil efficacy in endovascular surgeries.

Acknowledgments

The authors wish to thank Kari Habursky for technical assistance.

Abbreviations and Acronyms

cDNA	Complementary DNA
DEG	Differentially expressed gene
EC	Endothelial cell
ECM	Extracellular matrix

GDC	Guglielmi detachable coil
HUVEC	Human umbilical vein endothelial cell
IPA	Ingenuity Pathway Analysis
ISAT	International Subarachnoid Aneurysm Trial
PGLA	Polyglycolic acid

References

1. Babiker MH, Gonzalez LF, Albuquerque F, Collins D, Elvikis A, Frakes DH. Quantitative effects of coil packing density on cerebral aneurysm fluid dynamics: an in vitro steady flow study. Ann Biomed Eng. 2010; 38:2293–2301. [PubMed: 20306135]
2. Barry OP, Pratico D, Lawson JA, FitzGerald GA. Transcellular activation of platelets and endothelial cells by bioactive lipids in platelet microparticles. J Clin Invest. 1997; 99:2118–2127. [PubMed: 9151784]
3. Bavinzski G, Richling B, Binder BR, Gruber A, Talazoglu V, Dietrich W, Schwendtenwein I, Plenk H Jr. Histopathological findings in experimental aneurysms embolized with conventional and thrombogenic/antithrombolytic Guglielmi coils. Minim Invasive Neurosurg. 1999; 42:167–174. [PubMed: 10667819]
4. Bavinzski G, Talazoglu V, Killer M, Richling B, Gruber A, Gross CE, Plenk H Jr. Gross and microscopic histopathological findings in aneurysms of the human brain treated with Guglielmi detachable coils. J Neurosurg. 1999; 91:284–293. [PubMed: 10433317]
5. Cognard C, Weill A, Spelle L, Piotin M, Castaings L, Rey A, Moret J. Long-term angiographic follow-up of 169 intracranial berry aneurysms occluded with detachable coils. Radiology. 1999; 212:348–356. [PubMed: 10429689]
6. Frosen J, Piippo A, Paetau A, Kangasniemi M, Niemela M, Hernesniemi J, Jaaskelainen J. Remodeling of saccular cerebral artery aneurysm wall is associated with rupture: histological analysis of 24 unruptured and 42 ruptured cases. Stroke. 2004; 35:2287–2293. [PubMed: 15322297]
7. Furchgott RF, Zawadzki JV. The obligatory role of endothelial cells in the relaxation of arterial smooth muscle by acetylcholine. Nature. 1980; 288:373–376. [PubMed: 6253831]
8. Geyik S, Yavuz K, Ergun O, Koc O, Cekirge S, Saatci I. Endovascular treatment of intracranial aneurysms with bioactive Cerecyte coils: effects on treatment stability. Neuroradiology. 2008; 50:787–793. [PubMed: 18483727]
9. Hebert CA, Luscinskas FW, Kiely JM, Luis EA, Darbonne WC, Bennett GL, Liu CC, Obin MS, Gimbrone MA Jr, Baker JB. Endothelial and leukocyte forms of IL-8. Conversion by thrombin and interactions with neutrophils. J Immunol. 1990; 145:3033–3040. [PubMed: 2212672]
10. Kubota Y, Kawa Y, Mizoguchi M. CDw49b/CD29 integrin complex mediates the differentiation of human endothelial cells into capillary-like structures in vitro. J Dermatol Sci. 1996; 12:36–43. [PubMed: 8740459]
11. Linfante I, Akkawi NM, Perlow A, Andreone V, Wakhloo AK. Polyglycolide/polylactide-coated platinum coils for patients with ruptured and unruptured cerebral aneurysms: a single-center experience. Stroke. 2005; 36:1948–1953. [PubMed: 16051893]
12. Maciag T, Cerundolo J, Ilsley S, Kelley PR, Forand R. An endothelial cell growth factor from bovine hypothalamus: identification and partial characterization. Proc Natl Acad Sci U S A. 1979; 76:5674–5678. [PubMed: 293671]
13. McGuire PG, Orkin RW. Isolation of rat aortic endothelial cells by primary explant techniques and their phenotypic modulation by defined substrata. Lab Invest. 1987; 57:94–105. [PubMed: 3298852]
14. Mechtersheimer G, Barth T, Hartschuh W, Lehnert T, Moller P. In situ expression of beta 1, beta 3 and beta 4 integrin subunits in non-neoplastic endothelium and vascular tumours. Virchows Arch. 1994; 425:375–384. [PubMed: 7529618]

15. Molyneux A, Kerr R, Stratton I, Sandercock P, Clarke M, Shrimpton J, Holman R. International Subarachnoid Aneurysm Trial (ISAT) of neurosurgical clipping versus endovascular coiling in 2143 patients with ruptured intracranial aneurysms: a randomised trial. Lancet. 2002; 360:1267–1274. [PubMed: 12414200]
16. O'Hare AM, Fanning NF, Ti JP, Dunne R, Brennan PR, Thornton JM. HydroCoils, occlusion rates, and outcomes: a large single-center study. AJNR Am J Neuroradiol. 2010; 31:1917–1922. [PubMed: 20705703]
17. Ozawa T, Tamatani S, Koike T, Abe H, Ito Y, Soga Y, Hasegawa H, Morita K, Tanaka R. Histological evaluation of endothelial reactions after endovascular coil embolization for intracranial aneurysm. Clinical and experimental studies and review of the literature. Interv Neuroradiol. 2003; 9:69–82. [PubMed: 20591233]
18. Pandey AS, Koebbe C, Rosenwasser RH, Veznedaroglu E. Endovascular coil embolization of ruptured and unruptured posterior circulation aneurysms: review of a 10-year experience. Neurosurgery. 2007; 60:626–637. [PubMed: 17415199]
19. Panetta CJ, Miyauchi K, Berry D, Simari RD, Holmes DR, Schwartz RS, Caplice NM. A tissue-engineered stent for cell-based vascular gene transfer. Hum Gene Ther. 2002; 13:433–441. [PubMed: 11860710]
20. Plachokova A, Link D, van den Dolder J, van den Beucken J, Jansen J. Bone regenerative properties of injectable PGLA-CaP composite with TGF-beta1 in a rat augmentation model. J Tissue Eng Regen Med. 2007; 1:457–464. [PubMed: 18265419]
21. Sarrafzadeh A, Haux D, Kuchler I, Lanksch WR, Unterberg AW. Poor-grade aneurysmal subarachnoid hemorrhage: relationship of cerebral metabolism to outcome. J Neurosurg. 2004; 100:400–406. [PubMed: 15035274]
22. Stiver SI, Porter PJ, Willinsky RA, Wallace MC. Acute human histopathology of an intracranial aneurysm treated using Guglielmi detachable coils: case report and review of the literature. Neurosurgery. 1998; 43:1203–1208. [PubMed: 9802864]
23. Tamatani S, Ozawa T, Minakawa T, Takeuchi S, Koike T, Tanaka R. Histological interaction of cultured endothelial cells and endovascular embolic materials coated with extracellular matrix. J Neurosurg. 1997; 86:109–112. [PubMed: 8988088]
24. Tamatani S, Ozawa T, Minakawa T, Takeuchi S, Koike T, Tanaka R. Radiologic and histopathologic evaluation of canine artery occlusion after collagen-coated platinum microcoil delivery. AJNR Am J Neuroradiol. 1999; 20:541–545. [PubMed: 10319955]
25. Vance MM, Wiley LM. Gap junction intercellular communication mediates the competitive cell proliferation disadvantage of irradiated mouse preimplantation embryos in aggregation chimeras. Radiat Res. 1999; 152:544–551. [PubMed: 10521932]
26. Vittet D, Prandini MH, Berthier R, Schweitzer A, Martin-Sisteron H, Uzan G, Dejana E. Embryonic stem cells differentiate in vitro to endothelial cells through successive maturation steps. Blood. 1996; 88:3424–3431. [PubMed: 8896407]
27. Vu K, Weksler B, Romero I, Couraud PO, Gelli A. Immortalized human brain endothelial cell line HCMEC/D3 as a model of the blood-brain barrier facilitates in vitro studies of central nervous system infection by *Cryptococcus neoformans*. Eukaryot Cell. 2009; 8:1803–1807. [PubMed: 19767445]
28. Wu KK, Thiagarajan P. Role of endothelium in thrombosis and hemostasis. Annu Rev Med. 1996; 47:315–331. [PubMed: 8712785]
29. Yang D, Guo T, Nie C, Morris SF. Tissue-engineered blood vessel graft produced by self-derived cells and allogenic acellular matrix: a functional performance and histologic study. Ann Plast Surg. 2009; 62:297–303. [PubMed: 19240529]

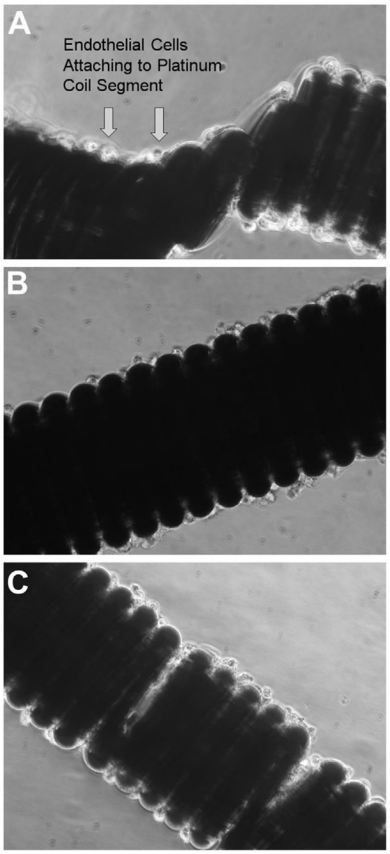

Figure 1.
Phase contrast photomicrographs showing endothelial cells attached to coil at day 1 (**A**), day 4 (**B**), and day 7 (**C**).

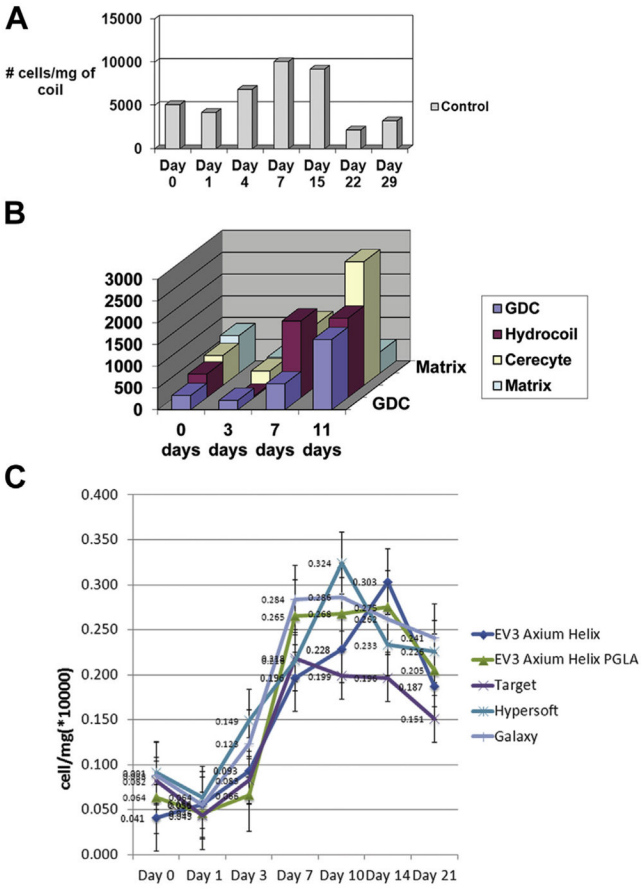

Figure 2.

Bar graphs illustrating human umbilical vein endothelial cell growth on platinum (**A**) and bioactive (**B**) coils. Human brain endothelial cell growth on platinum-based coil surfaces per mg of coil (**C**). GDC, Guglielmi detachable coil; PGLA, polyglycolic acid.

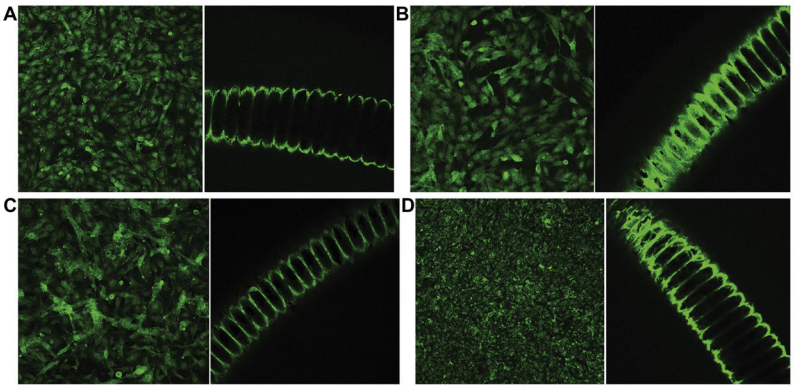

Figure 3.

Control (*left*) and experimental (*right*) immunohistochemical staining for α_1 integrin (**A**), α_2 integrin (**B**), β_1 integrin (**C**), and platelet endothelial cell adhesion molecule (**D**) showing endothelial cell localization on coils. Control images represent staining of cells attached to the surface of the wells rather than the coil segments.

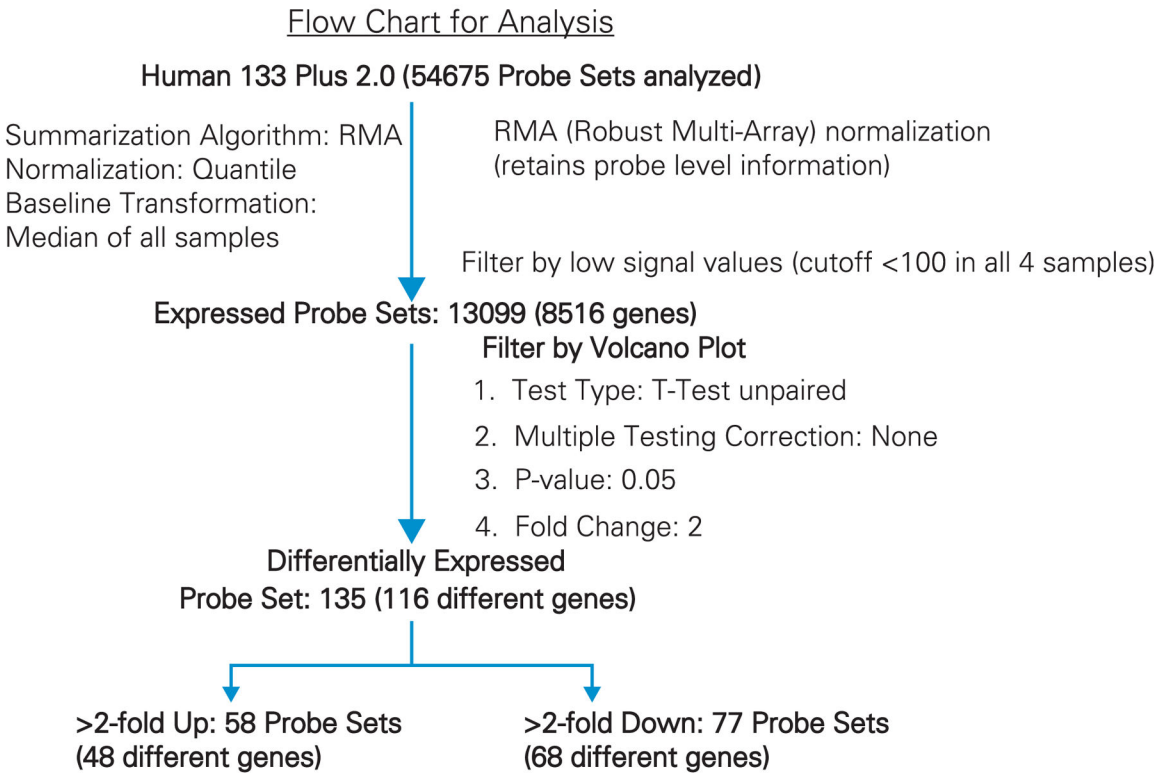

Figure 4.
Flow chart analysis of gene expression.

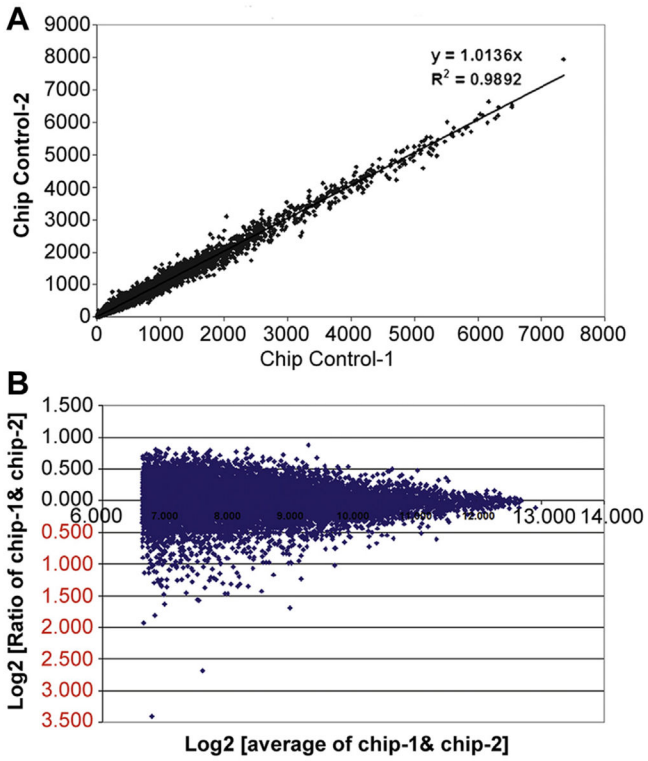

Figure 5.

Scatter plots used to define array reproducibility. (**A**) Gene expression intensities from microarrays using duplicate control cultures (self versus self-experiment). (**B**) Log scatter plot (control self-experiment). Signal values are graphed from all probe sets on the two arrays, each hybridized with one of two duplicate untreated sample targets.

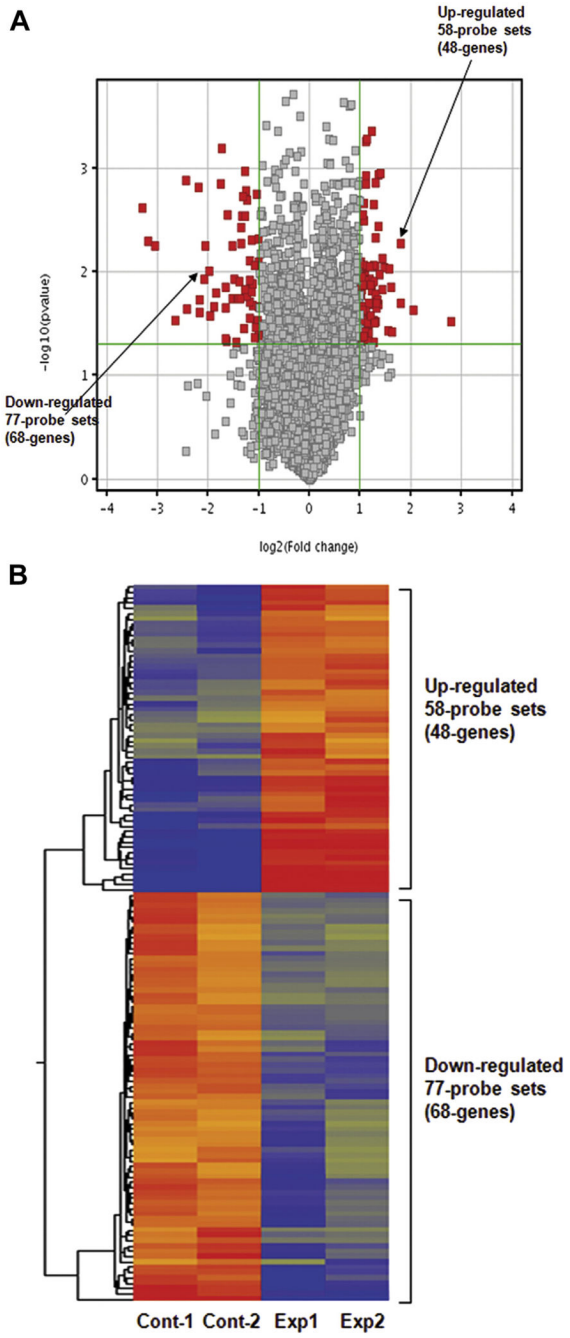

Figure 6.

(**A**) Volcano plot showing differentially expressed genes (135 differentially expressed probe set; 116 genes). Relationship between fold-change (>2; magnitude of change; x-axis) and statistical significance (P = 0. 05; y-axis) is shown. (**B**) Heat map from microarray data reflecting gene expression comparing four different samples: two controls and two coil-treated cultures.

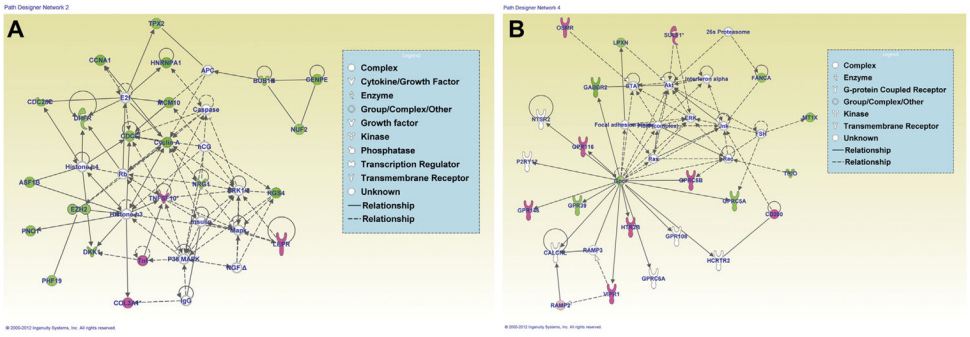

Figure 7.

Network analysis using Ingenuity Pathway Analysis (IPA). IPA analysis from differentially expressed genes shows predominant networks affected. (**A**) Cellular assembly and organization, cell cycle, cell morphology (*green* indicates down-regulated, *pink* represents up-regulated genes). (**B**) Cell signaling, nucleic acid metabolism, small molecule biochemistry.

Table 1

Down-Regulated Gene List

Probe Set ID	Gene Symbol	Gene Title	Fold Change	Control	Experimental
239331_at		Transcribed locus	0.151	139	21
232174_at		CDNA: FLJ21635 fis, clone COL08233, highly similar to AF131819 *Homo sapiens* clone 24838 mRNA sequence	0.245	323	79
222040_at	HNRNPA1///LOC728844	Heterogeneous nuclear ribonucleoprotein A1///hypothetical LOC728844	0.288	125	36
230127_at		Transcribed locus	0.293	167	49
227165_at	C13orf3	Chromosome 13 open reading frame 3	0.331	118	39
209990_s_at	GABBR2	Gamma-aminobutyric acid (GABA) B receptor, 2	0.331	136	45
215100_at	C6orf105	Chromosome 6 open reading frame 105	0.339	112	38
207526_s_at	IL1RL1	Interleukin 1 receptor-like 1	0.341	464	158
204338_s_at	RGS4	Regulator of G-protein signaling 4	0.361	108	39
221521_s_at	GINS2	GINS complex subunit 2 (Psf2 homolog)	0.370	211	78
205899_at	CCNA1	Cyclin A1	0.371	510	189
205681_at	BCL2A1	BCL2-related protein A1	0.378	172	65
204817_at	ESPL1	Extra spindle pole bodies homolog 1 (*S. cerevisiae*)	0.380	92	35
201506_at	TGFBI	Transforming growth factor, beta-induced, 68 kDa	0.391	128	50
205576_at	SERPIND1	Serpin peptidase inhibitor, clade D (heparin cofactor), member 1	0.391	391	153
235425_at	SGOL2	Shugoshin-like 2 (*S. pombe*)	0.392	158	62
234066_at	IL1RL1	Interleukin 1 receptor-like 1	0.395	233	92
226695_at	PRRX1	Paired related homeobox 1	0.403	124	50
235236_at		Transcribed locus	0.404	171	69
207601_at	SULT1B1	Sulfotransferase family, cytosolic, 1B, member 1	0.404	314	127
225239_at		CDNA FLJ26120 fis, clone SYN00419	0.407	280	114
205046_at	CENPE	Centromere protein E, 312 kDa	0.407	194	79
231403_at	TRIO	Triple functional domain (PTPRF interacting)	0.407	108	44
220940_at	ANKRD36B	Ankyrin repeat domain 36B	0.408	179	73
217165_x_at	MT1F	Metallothionein 1F	0.408	218	89
220651_s_at	MCM10	Minichromosome maintenance complex component 10	0.412	102	42

Probe Set ID	Gene Symbol	Gene Title	Fold Change	Control	Experimental
229610_at	CKAP2L	Cytoskeleton-associated protein 2-like	0.415	224	93
204823_at	NAV3	Neuron navigator 3	0.415	426	177
226419_s_at	FLJ44342	Hypothetical LOC645460	0.416	377	157
204602_at	DKK1	Dickkopf homolog 1 (*Xenopus laevis*)	0.422	446	188
213684_s_at	PDLIM5	PDZ and LIM domain 5	0.424	125	53
212020_s_at	MKI67	Antigen identified by monoclonal antibody Ki-67	0.426	141	60
201195_s_at	SLC7A5	Solute carrier family 7 (cationic amino acid transporter, y+ system), member 5	0.429	392	168
230082_at	LOC100133660	Hypothetical LOC100133660	0.432	95	41
221436_s_at	CDCA3	Cell division cycle associated 3	0.434	143	62
221685_s_at	CCDC99	Coiled–coil domain containing 99	0.435	308	134
218009_s_at	PRC1	Protein regulator of cytokinesis 1	0.437	421	184
242809_at	IL1RL1	Interleukin 1 receptor-like 1	0.439	611	268
218115_at	ASF1B	ASF1 anti-silencing function 1 homolog B (S. cerevisiae)	0.444	169	75
212021_s_at	MKI67	Antigen identified by monoclonal antibody Ki-67	0.447	132	59
220865_s_at	PDSS1	Prenyl (decaprenyl) diphosphate synthase, subunit 1	0.448	125	56
203968_s_at	CDC6	Cell division cycle 6 homolog (*S. cerevisiae*)	0.451	122	55
219148_at	PBK	PDZ binding kinase	0.455	321	146
212023_s_at	MKI67	Antigen identified by monoclonal antibody Ki-67	0.455	134	61
203108_at	GPRC5A	G protein-coupled receptor, family C, group 5, member A	0.459	196	90
204326_x_at	MT1X	Metallothionein 1X	0.461	206	95
210052_s_at	TPX2	TPX2, microtubule-associated, homolog (*Xenopus laevis*)	0.464	466	216
219557_s_at	NRIP3	Nuclear receptor interacting protein 3	0.466	131	61
205167_s_at	CDC25C	Cell division cycle 25 homolog C (S. pombe)	0.467	120	56
218663_at	NCAPG	Non-SMC condensin I complex, subunit G	0.467	345	161
203622_s_at	PNO1	Partner of NOB1 homolog (*S. cerevisiae*)	0.470	117	55
218355_at	KIF4A	Kinesin family member 4A	0.473	510	241
206343_s_at	NRG1	Neuregulin 1	0.475	101	48
239202_at		CDNA FLJ34848 fis, clone NT2NE2011684, weakly similar to *H. sapiens* mRNA for plakophilin 2a and b	0.477	239	114
206224_at	CST1	Cystatin SN	0.477	1404	670

World Neurosurg. Author manuscript; available in PMC 2015 November 01.

Probe Set ID	Gene Symbol	Gene Title	Fold Change	Control	Experimental
202016_at	MEST	Mesoderm specific transcript homolog (mouse)	0.477	220	105
222958_s_at	DEPDC1	DEP domain containing 1	0.478	301	144
239973_at		Transcribed locus	0.479	119	57
208600_s_at	GPR39	G protein-coupled receptor 39	0.480	667	320
226210_s_at	MEG3	Maternally expressed 3	0.480	175	84
227211_at	PHF19	PHD finger protein 19	0.483	236	114
219918_s_at	ASPM	asp (abnormal spindle) homolog, microcephaly associated (*Drosophila*)	0.484	411	199
219493_at	SHCBP1	SHC SH2-domain binding protein 1	0.486	144	70
213007_at	FANCI	Fanconi anemia, complementation group I	0.487	388	189
229070_at	C6orf105	Chromosome 6 open reading frame 105	0.487	956	466
203805_s_at	FANCA	Fanconi anemia, complementation group A	0.489	94	46
203358_s_at	EZH2	Enhancer of zeste homolog 2 (*Drosophila*)	0.491	330	162
223381_at	NUF2	NUF2, NDC80 kinetochore complex component, homolog (*S. cerevisiae*)	0.491	234	115
203438_at	STC2	Stanniocalcin 2	0.495	186	92
209714_s_at	CDKN3	Cyclin-dependent kinase inhibitor 3 (CDK2-associated dual specificity phosphatase)	0.497	290	144
212022_s_at	MKI67	Antigen identified by monoclonal antibody Ki-67	0.499	517	258
202533_s_at	DHFR	Dihydrofolate reductase	0.500	134	67
203755_at	BUB1B	BUB1 budding uninhibited by benzimidazoles 1 homolog beta (yeast)	0.500	416	208
206653_at	POLR3G	Polymerase (RNA) III (DNA directed) polypeptide G (32kD)	0.500	326	163
221520_s_at	CDCA8	Cell division cycle associated 8	0.500	170	85
205909_at	POLE2	Polymerase (DNA directed), epsilon 2 (p59 subunit)	0.502	231	116
216250_s_at	LPXN	Leupaxin	0.503	163	82

Table 2

Up-Regulated Gene List

Probe Set ID	Gene Symbol	Gene Title	Fold Change	Control	Experimental
227235_at		CDNA clone IMAGE:5302158	9.887	11	113
222106_at	PRND	Pprion protein 2 (dublet)	9.071	39	356
202350_s_at	MATN2	Matrilin 2	8.284	18	149
209392_at	ENPP2	Ectonucleotide pyrophosphatase/phosphodiesterase 2 (autotaxin)	6.284	12	80
214180_at	MAN1C1	Mannosidase, alpha, class 1C, member 1	5.427	27	144
217757_at	A2M	Alpha-2-macroglobulin	5.347	31	161
212344_at	SULF1	Sulfatase 1	4.597	60	274
201852_x_at	COL3A1	Collagen, type III, alpha 1 (Ehlers-Danlos syndrome type IV, autosomal dominant)	4.504	46	203
215076_s_at	COL3A1	Collagen, type III, alpha 1 (Ehlers-Danlos syndrome type IV, autosomal dominant)	4.498	45	197
201150_s_at	TIMP3	TIMP metallopeptidase inhibitor 3 (Sorsby fundus dystrophy, pseudoinflammatory)	4.227	43	182
209047_at	AQP1	Aquaporin 1 (Colton blood group)	4.158	84	346
201009_s_at	TXNIP	Thioredoxin interacting protein	3.936	54	211
204904_at	GJA4	Gap junction protein, alpha 4, 37kDa	3.92	36	137
203423_at	RBP1	Retinol binding protein 1, cellular	3.696	75	274
211161_s_at	COL3A1	Collagen, type III, alpha 1 (Ehlers-Danlos syndrome type IV, autosomal dominant)	3.605	159	582
201148_s_at	TIMP3	TIMP metallopeptidase inhibitor 3 (Sorsby fundus dystrophy, pseudoinflammatory)	3.387	55	187
209543_s_at	CD34	CD34 molecule	3.339	103	343
40687_at	GJA4	Gap junction protein, alpha 4, 37 kDa	3.18	42	133
206638_at	HTR2B	5-hydroxytryptamine (serotonin) receptor 2B	3.177	104	330
212353_at	SULF1	Sulfatase 1	3.177	177	566
201262_s_at	BGN	Biglycan	3.125	114	345
209583_s_at	CD200	CD200 molecule	3.067	33	101
228770_at	GPR146	G protein-coupled receptor 146	2.893	75	216
201010_s_at	TXNIP	Thioredoxin interacting protein	2.792	160	447
205019_s_at	VIPR1	Vasoactive intestinal peptide receptor 1	2.722	36	96
202688_at	TNFSF10	Tumor necrosis factor (ligand) superfamily, member 10	2.693	197	535
209182_s_at	C10orf10	Chromosome 10 open reading frame 10	2.657	189	499

Probe Set ID	Gene Symbol	Gene Title	Fold Change	Control	Experimental
209894_at	LEPR	Leptin receptor	2.632	48	127
227243_s_at	EBF3	Early B-cell factor 3	2.579	41	105
226237_at		mRNA full length insert cDNA clone EUROIMAGE 1913076	2.562	139	358
205779_at	RAMP2	Receptor (G protein-coupled) activity modifying protein 2	2.546	52	133
217897_at	FXYD6	FXYD domain containing ion transport regulator 6	2.529	93	235
238673_at	SAMD12	Sterile alpha motif domain containing 12	2.494	61	151
226621_at		Transcribed locus	2.458	124	308
216598_s_at	CCL2	Chemokine (C-C motif) ligand 2	2.433	545	1326
214329_x_at	TNFSF10	Tumor necrosis factor (ligand) superfamily, member 10	2.422	63	151
219304_s_at	PDGFD	Platelet derived growth factor D	2.421	45	108
202838_at	FUCA1	Fucosidase, alpha-L- 1, tissue	2.391	59	141
202291_s_at	MGP	Matrix Gla protein	2.376	543	1291
212354_at	SULF1	Sulfatase 1	2.352	547	1292
230740_at		Transcribed locus	2.284	92	210
202947_s_at	GYPC	Glycophorin C (Gerbich blood group)	2.278	62	142
224818_at	SORT1	Sortilin 1	2.275	54	122
227306_at		CDNA: FLJ21245 fis, clone COL01184	2.26	44	99
223449_at	SEMA6A	Sema domain, transmembrane domain (TM), and cytoplasmic domain, (semaphorin) 6A	2.223	145	322
225511_at	GPRC5B	G protein-coupled receptor, family C, group 5, member B	2.203	113	249
203498_at	RCAN2	Regulator of calcineurin 2	2.192	85	186
202023_at	EFNA1	Ephrin-A1	2.179	184	398
227040_at	NHLRC3	NHL repeat containing 3	2.114	43	91
240890_at	LOC643733	Hypothetical LOC643733	2.113	370	782
235887_at		Transcribed locus	2.088	44	93
204358_s_at	FLRT2	Fibronectin leucine rich transmembrane protein 2	2.079	140	291
218999_at	TMEM140	Transmembrane protein 140	2.039	130	265
212951_at	GPR116	G protein-coupled receptor 116	2.023	107	217
213894_at	THSD7A	Thrombospondin, type I, domain containing 7A	2.021	69	140
218966_at	MYO5C	Myosin VC	2.021	259	526

Probe Set ID	Gene Symbol	Gene Title	Fold Change	Control	Experimental
212325_at	LIMCH1	LIM and calponin homology domains 1	2.007	56	113

Table 3

Selected Networks with High Scores for Differentially Expressed Genes

Network	Molecules in Network	Score	Focus Molecules	Top Functions
1	A2M, Alp, Ap1, AQP1, BCL2A1, BGN, CCL2, CD34, CDKN3, Collagen type I, Collagen(s), EFNA1, FUCA1, IL1, IL1RL1, KIF4A, LDL, MKI67, Mmp, MT1F, NCAPG, NFkB, PBK, Pdgf, PDGF BB, PDGFD, PRC1, PRRX1, RBP1, SERPIND1, Tgf beta, TGFBI, TIMP3, TXNIP, Vegf	48	23	Connective tissue disorders, infectious disease, inflammatory disease
2	APC, ASF1B, BUB1B, Caspase, CCNA1, CDC6, CDC25C, CENPE, COL3A1, Cyclin A, DHFR, DKK1, E2f, ERK1/2, EZH2, hCG, Histone h3, Histone h4, HNRNPA1, IgG, Insulin, LEPR, Mapk, MCM10, NGF, NRG1, NUF2, P38 MAPK, PHF19, PNO1, Rb, RGS4, Tnf, TNFSF10, TPX2	40	20	Cellular assembly and organization, cell cycle, cell morphology
3	AMBP, AQP1, ASPM, butyric acid, C10ORF10, CCDC99, CDC14B, DEPDC1, EHD1, EHD3, ENPP2, FANCI, FXYD6, GINS2, HMGN2, HNF4A, IFITM2, KNTC1, L-triiodothyronine, LIMCH1, LZTR1, MEG3, MIR124, PELO, PODXL, POLR3G, RCAN2, SULT1B1, TGFBI, THSD7A, TMEM140, TNF, TP53, WTAP, ZNF224	34	18	Gene expression, infection mechanism, cellular development
4	26s Proteasome, Akt, CALCRL, CD200, ERK, FANCA, Focal adhesion kinase, FSH, GABBR2, Gpcr, GPR39, GPR108, GPR116, GPR146, GPRC5A, GPRC5B, GPRC6A, HCRTR2, HTR2B, Interferon alpha, Jnk, LPXN, MT1X, NTSR2, OSMR, P2RY12, PI3K, Rac, RAMP2, RAMP3, Ras, STAT, SULF1, TRIO, VIPR1	30	16	Cell signaling, nucleic acid metabolism, small molecule biochemistry
5	ADAM12, ADCY3, ANKRD36B, ARAP1, ASPM, BDKRB1, C5ORF13, Ca2+, CDCA3, CLTC, EBF3, EHD1, ESPL1, GLI1, GYPC, KDM5B, MAN1C1, MEST, MPP1, NAV3, PDLIM5, PLOD1, PRC1, PRND, PTH1R, RTKN2, SEMA6A, SERPINH1, SH3D19, SHCBP1, SLC2A4, SMAD2, TGFB1, TGFBR3, TUFM	25	14	Cardiovascular system development and function, organismal development, tissue morphology

Table 4

Molecular and Cellular Functions of Differentially Expressed Genes

Functions	Number of Molecules
Cellular growth and proliferation	46
Cell cycle	26
Cellular assembly and organization	18
Cellular movement	23
Cell morphology	13
Cell-to-cell signaling and interaction	19